Journal of Alloys and Compounds 505 (2010) 201–205

Contents lists available at ScienceDirect

Journal of Alloys and Compounds

journal homepage: www.elsevier.com/locate/jallcom

Alloying behavior of erbium in an Al–Cu–Mg alloy

Xu Chen[a,b], Zhiyi Liu[a,b,*], Song Bai[a,b], Yao Li[a,b], Lianghua Lin[a,b]

[a] Key Laboratory of Nonferrous Metal Materials Science and Engineering, Ministry of Education, Central South University, Changsha 410083, People's Republic of China
[b] School of Material Science and Engineering, Central South University, Changsha 410083, People's Republic of China

ARTICLE INFO

Article history:
Received 29 November 2009
Received in revised form 4 June 2010
Accepted 10 June 2010
Available online 16 June 2010

Keywords:
Erbium
Al_8Cu_4Er phase
Al_3Er phase
Al–Cu–Mg alloy

ABSTRACT

The alloying behavior of rare earth erbium in an Al–Cu–Mg alloy was characterized by employing OM, SEM, EDS, XRD and TEM. The results suggested the erbium mainly segregated to the grain boundaries in a form of Al_8Cu_4Er phase during solidification, which was crushed up along with the grain boundaries after hot rolling. Moreover, Al_3Er phase with the $L1_2$ structure was also observed in the Al–Cu–Mg–Er alloy in T351 condition. The dendritic structure of as-cast Al–Cu–Mg alloy was refined remarkably by erbium addition.

1. Introduction

It is well known that small additions of rare earth elements are of great importance to improve the mechanical properties of Al-based alloys [1–5]. Over the past several years, scandium (Sc) has been most commonly studied as microalloying element in the case of Al-based alloys, indicating the beneficial effects on mechanical properties that associated remarkably with grain refinement, dynamic recrystallization controlling and enhanced strength because of the existence of coherent Al_3Sc precipitates [6–12]. However, the applications of Sc-bearing alloys are extremely restricted due to the high cost of Sc addition. Instead, much attention has been focused on rare earth erbium (Er), which is much cheaper than Sc [4,13]. The equilibrium precipitate of Al_3Er phase can be decomposed from the Al–Er solid solution during heat treatment and is coherent or semi-coherent to the aluminum matrix [14]. Furthermore, Al_3Er phase also has high melting point and thermal stability [15].

Although the solid solubility of erbium in α-Al (0.046 at.% Er at 640 °C [16]) is low, Al_3Er phase was still detected in many aluminum alloys. Ruder and Eliezer [14] found the Er mainly existed in the Al_3Er phase in the Al–4Er alloy and the orientation relationships between the matrix and the dispersed phase are $\{100\}_{Al_3Er}||\{100\}_{Al}$; $\langle 100\rangle$ $Al_3Er||\langle 100\rangle_{Al}$. Based on the research by Karnesky et al. [13], Er seized the position of Sc up to at least 30% in crystal lattice of near-stoichiometric $Al_3(Sc_{1-x}Er_x)$ precipitates with the $L1_2$ structure in Al–0.06Sc–0.02Er (at.%) alloy, suggesting Er can replace the more expensive Sc in the precipitates. Many investigations also found the Al_3Er phase present in Al–5Mg–1Er alloy [17], Al–4.5Mg–0.7Mn–0.1Zr–0.6Er alloy [18], 5083 alloy [19] and A1–6Zn–2Mg–0.4Er alloy [20]. Mao et al. [21] demonstrated that both Al_3Er phase and ternary AlCuEr phase were present in Al–5.91Zn–1.81Mg–1.78Cu–0.22Er alloy. However, it is worth of noting that erbium mainly segregated at the grain boundary in a form of ternary Al_8Cu_4Er phase in Al–4.66Cu–0.39Mg–0.13Zr–0.28Er alloy, no Al_3Er phase was found as proposed by Li et al. [22].

As one of the most effective additions, investigations related to the alloying behavior of erbium in aluminum alloys have been studied for many years, but the effects of erbium in the Al–Cu–Mg alloys still need to be understood in detail and up till now no previous work was conducted to report the present of the Al_3Er phase in the alloy. Therefore, Al–4.1Cu–1.37Mg–0.2Er alloy without Zr and Sc additions was employed in present work to clarify the alloying behavior of erbium in the Al–Cu–Mg alloy.

2. Experimental

The chemical compositions of the alloys, i.e., the base alloy 2524 (hereafter termed the Al–Cu–Mg alloy) and the base alloy containing Er (hereafter termed the Al–Cu–Mg–Er alloy) investigated are given in Table 1. The alloys were prepared in an electrical resistance furnace and iron mold casting. Al (99.99 wt.%) was produced by Xinjiang Joinworld Co. Ltd. and was found that Fe and Si are not in excess of 0.0024 wt.% and 0.0023 wt.%, respectively. The rest alloying elements were added in the form of Al base master alloys. An Al–24.8 wt.% Er master alloy was provided by Hunan Rare Earth Metal and Material Institute. Al–10 wt.%Mn and Al–4 wt.%Ti

* Corresponding author at: School of Material Science and Engineering, Central South University, Changsha 410083, People's Republic of China.
Tel.: +86 731 88836011; fax: +86 731 88876692.
E-mail address: liuzhiyi@mail.csu.edu.cn (Z. Liu).

0925-8388/$ – see front matter.
doi:10.1016/j.jallcom.2010.06.029

Table 1
Chemical compositions of the Al–Cu–Mg–(Er) alloys (wt.%).

Alloy	Cu	Mg	Mn	Ti	Er	Fe	Si	Al
Er-free	4.14	1.34	0.51	0.09	0	0.03	0.02	Bal.
Er-containing	4.10	1.37	0.52	0.10	0.20	0.04	0.02	Bal.

master alloy were produced by Southwest Aluminum Co. Ltd. The Al–49.5 wt.%Cu master alloy was produced by electrical resistance furance from 99.99 wt.% Al and 99.99 wt.% Cu (Daye Nonferrous Metals Group). The as-cast materials were then characterized to examine the morphology and the compositions of the phase particles of interest. The ingots were homogenized for 24 h at 480 °C which is below the eutectic temperature and subsequently hot rolled to sheets of about 3 mm thickness.

Specimens for microstructure examination were prepared from the as-cast and hot rolled samples in conventional way. The optical microscopy (OM) together with scanning electron microscopy (SEM) were employed to reveal the typical features. A FEI Quanta 200 scanning electron microscope equipped with EDAX Genesis (EDS) machine was used in studying the morphology and chemical compositions of the phases in the alloy. The operating voltage of the SEM was 20 kV. The scanning electron micrographs presented in this investigation were taken in the back scattered electron imaging mode to facilitate identification of the particles. The elements mapping was carried out in order to determine the distributions of the alloying elements, especially erbium. All the analyses using SEM were carried out on polished but unetched samples. Phases constitution analyses of the as-cast alloy were further performed with X-ray diffraction patterns generated by a Rigaku RINT D/Max-2500 with Cu k_α-radiation.

Vickers microhardness was measured on polished samples using the average value from at least 10 independent measurements with a load of 3 kg. Slices for transmission electron microscopy (TEM) samples were cut from the plate in T351 condition (solution heat treated, stretched, and naturally aged), and were subsequently ground to 100 μm and punched into 3 mm disc. The electrolyte was a mixture of 70% methanol and 30% nitric acid, and thinning was performed at −25 °C. TEM observation was carried out on a TecnaiG^{2}20 TEM machine with an operating voltage of 200 kV.

3. Results and discussion

3.1. As-cast structure

The optical microstructures of the as-cast Al–Cu–Mg(–Er) alloys were characterized in order to reveal the influence of erbium addition as shown in Fig. 1, which illustrates that the addition of rare earth erbium refine the as-cast structure of Al–Cu–Mg alloy apparently. The typical grain structure of the Al–Cu–Mg alloy that predominated by large equiaxed grains with the average grain size is about 100 μm as shown in Fig. 1(a), and a small amount of dendritic structures are also visible. On the contrary, the as-cast structure of the Al–Cu–Mg–Er alloy is dominated by coarsening dendrites and the grain boundaries are decorated by continuous phases in Fig. 1(b). Moreover, the distance between the branches of the dendritic structure is about 45 μm, which in fact displays a decrease compared to Al–Cu–Mg alloy. Obviously, Er added to the Al–Cu–Mg alloy refined the α-Al grains and inhabited the growth of the dendritic structures.

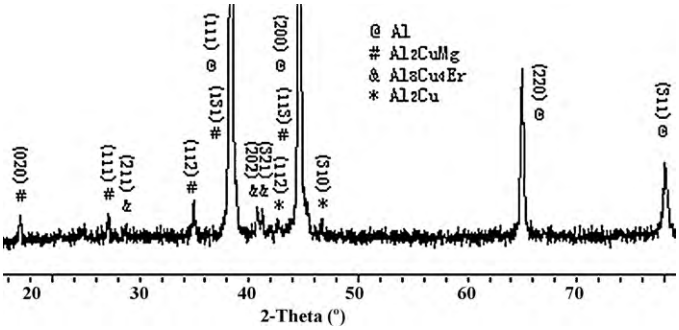

Fig. 2. X-ray diffraction pattern of the as-cast Al–Cu–Mg–Er alloy.

Table 2
Compound compositions at grain boundaries of the as-cast Al–Cu–Mg–Er alloy by EDS (at.%).

Position	Al	Cu	Mg	Er	Mn
A	71.9	16.4	1.7	4.1	5.9
B	72.4	14.8	12.8	0	0
C	71.1	23.8	5.1	0	0
D	71.0	29.0	0	0	0

3.2. Phase constitution

The experimental alloys are based on Al–Cu–Mg system alloys and the mass ratio of Cu:Mg is approximately 3. According to the ternary Al–Cu–Mg phase diagram [23], the composition of the base alloy just lies within (α + θ + S) phase field. Fig. 2 represents the X-ray diffraction pattern of the as-cast Al–Cu–Mg–Er alloy examined in this investigation which indicates the existence of four phases. The XRD analysis revealed the presence of the three main phases (α-Al, θ-Al_2Cu and S-Al_2CuMg) and this finding is coincident with the Al–Cu–Mg phase diagram. In addition to the main three phases, Al_8Cu_4Er phase was also detected in the results of XRD analysis.

The backscattered electron images of the as-cast Al–Cu–Mg–Er alloy are illustrated in Fig. 3. It can be observed that the microstructures of as-cast ingots are dominated by dendritic α-Al and interdendritic eutectic structure. The dark areas are primary solid solution and some coarse bright particles are present at the grain boundaries, as shown in Fig. 3(a). The microstructures of the typical eutectic structure and the coarse second particles at higher magnification are given in Fig. 3(b) and (c). Moreover, the EDS analysis revealed these particles are of four different types, marked by A, B, C in Fig. 3(b) and D in Fig. 3(c), respectively. The chemical compositions of the phases are listed in Table 2.

A coarse bright phase was detected in the eutectic structure, marked by A in Fig. 3(b). According to the results of the analysis

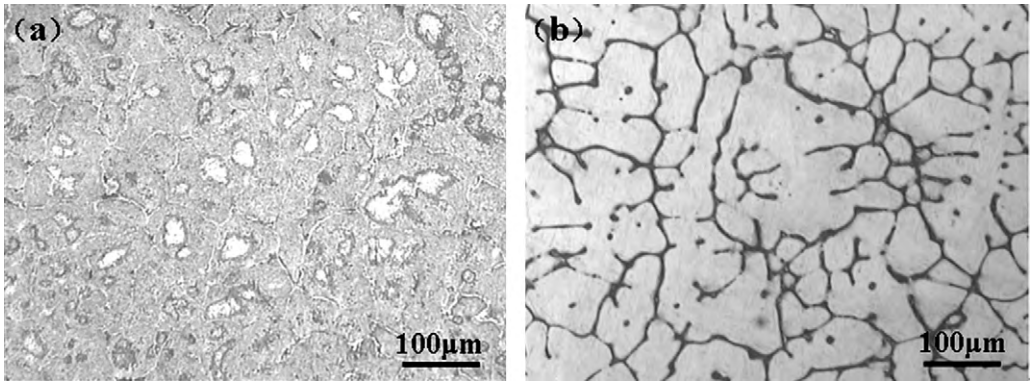

Fig. 1. The optical microstructures of as-cast alloys (a) Al–Cu–Mg alloy and (b) Al–Cu–Mg–Er alloy.

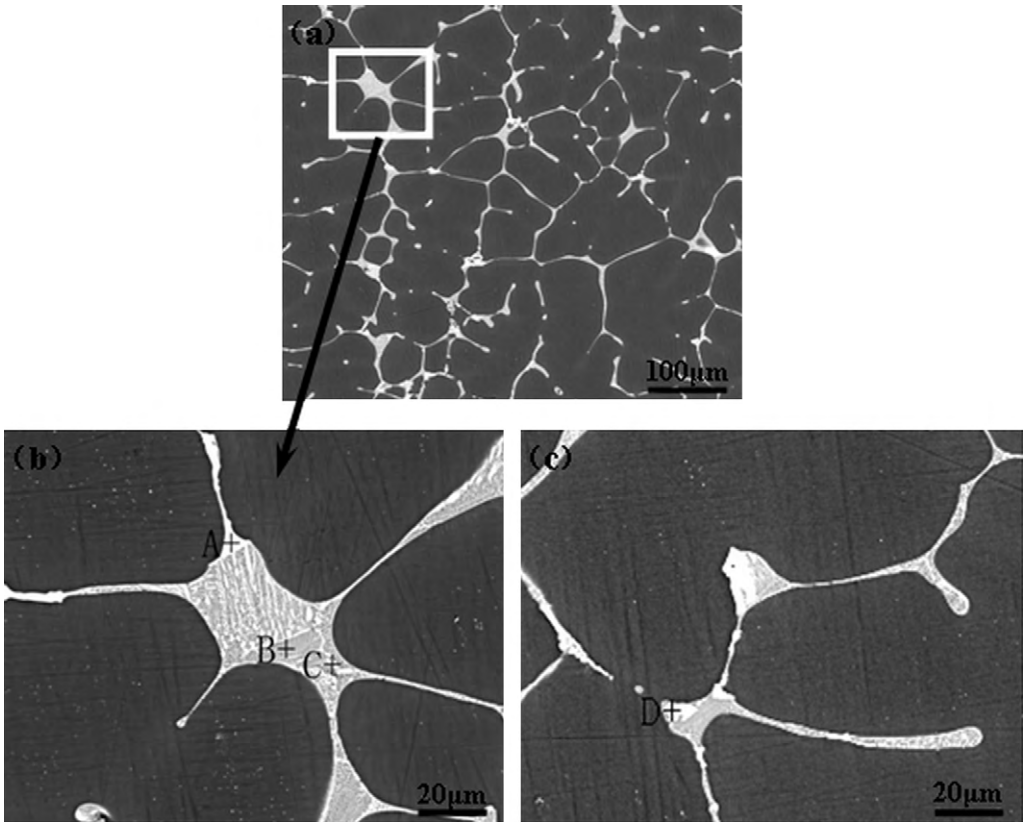

Fig. 3. Backscattered electron images of the as-cast Al–Cu–Mg–Er alloy. (a) Low magnification; (b) high magnification of the eutectic structure; and (c) coarse second phases.

by EDS, the bright particle is rich in erbium and the mol ratio of the Cu:Er is approximately 4:1, which is consistent with the ratio in Al_8Cu_4Er phase as the analysis of XRD in the present alloy in Fig. 2. The particle may be considered as Al_8Cu_4Er phase which is enriched by Mn. The apparent presence of excess amounts of Al in the particle is due to the matrix contribution to the analysis. Furthermore, it should be noticed that the nucleation sites of the Al_8Cu_4Er phase, as shown in Fig. 3, were always close to the interface of the α-Al phase and the interdendritic eutectic phase. Based on the Al–Cu–Er phase diagram [24], the solid solubility of erbium is relatively low at room temperature in aluminum alloys. Therefore, the concentration of erbium at the interface of the solid/liquid phases was certain to increase correspondingly during the solidification proceeds. The concentration fluctuation at the solid/liquid interface increased the constitutional undercooling, which leads to the grain refinement and the formation of Al_8Cu_4Er phase in the as-cast alloy [22].

The eutectic structures are present as lamellar structure in Fig. 3(b) and two types of different phases can also be tested marked by C and B, respectively. The gray phase in eutectic structure marked by B, is found to have the following composition: 14.8 at.% Cu, 12.8 at.% Mg and balance Al. From the XRD result, the presence of Al_2CuMg phase in the as-cast Al–Cu–Mg–Er alloy is obvious. The contents of Cu and Mg in this particle are, therefore, consistent with those of the S phase (Al_2CuMg) observed in the Al–Cu–Mg alloy. The more contribution of copper in EDS result should be ascribed to the interference by the bright phase in the eutectic structure. The bright phase in the eutectic structure marked by C, is found to have the following composition: 23.8 at.% Cu, 5.1 at.% Mg and balance Al. It seems that the bright phase is rich in copper compared to the S phase, which may mainly consist of Al_2Cu phase.

Another type of coarse bright phase [marked by D in Fig. 3(c)], other than the Al_8Cu_4Er phase, is found at the grain boundary in the as-cast Al–Cu–Mg–Er alloy and have the following composition: 29.0 at.% Cu and balance Al, as seen from Table 2. Therefore, the bright phase could be identified as Al_2Cu phase according to the EDS result, which agrees with the analysis of XRD.

To further understand the distribution of rare earth erbium in the experimental as-cast Al–Cu–Mg–Er alloy, the elements mapping of Al, Cu, Mg and Er were performed as shown in Fig. 4 which illustrated that erbium mostly distributed at the grain boundaries as ternary Al_8Cu_4Er phase. It is interesting to note that erbium is detected in the majority of the bright phases presented at the grain boundaries and there are two different types of bright phases at the grain boundaries, the Al_8Cu_4Er phase and Al_2Cu phase, respectively. Besides, the distributions of Cu and Mg coincide with the phase constitution containing Cu and Mg.

The optical microstructure of the hot rolled plate of Al–Cu–Mg–Er alloy along the longitudinal directions is represented in Fig. 5(a), suggesting that the coarse particles were crushed up along with the grain boundaries after hot rolling. The backscattered electron image of the hot rolled plate is given in Fig. 5(b) and the compositions of the undissolved phases [marked by E and F] were measured by EDS. The phase marked by E is found to have the following composition: 12.5 at.% Cu, 12.1 at.% Mg and balance Al [as shown in Table 3], which is consistent with the S phase. Furthermore, the bright phase marked by F could be identified as Al_8Cu_4Er phase according to the EDS result. After the obtained homogenization treatment in this investigation, Al_2CuMg phase and Al_8Cu_4Er phase cannot be redissolved into aluminum matrix sufficiently.

Table 3
Compound compositions of the phases in hot rolling Al–Cu–Mg–Er alloy by EDS (at.%).

Position	Al	Cu	Mg	Er
E	75.4	12.5	12.1	0
F	65.4	30.1	0	4.5

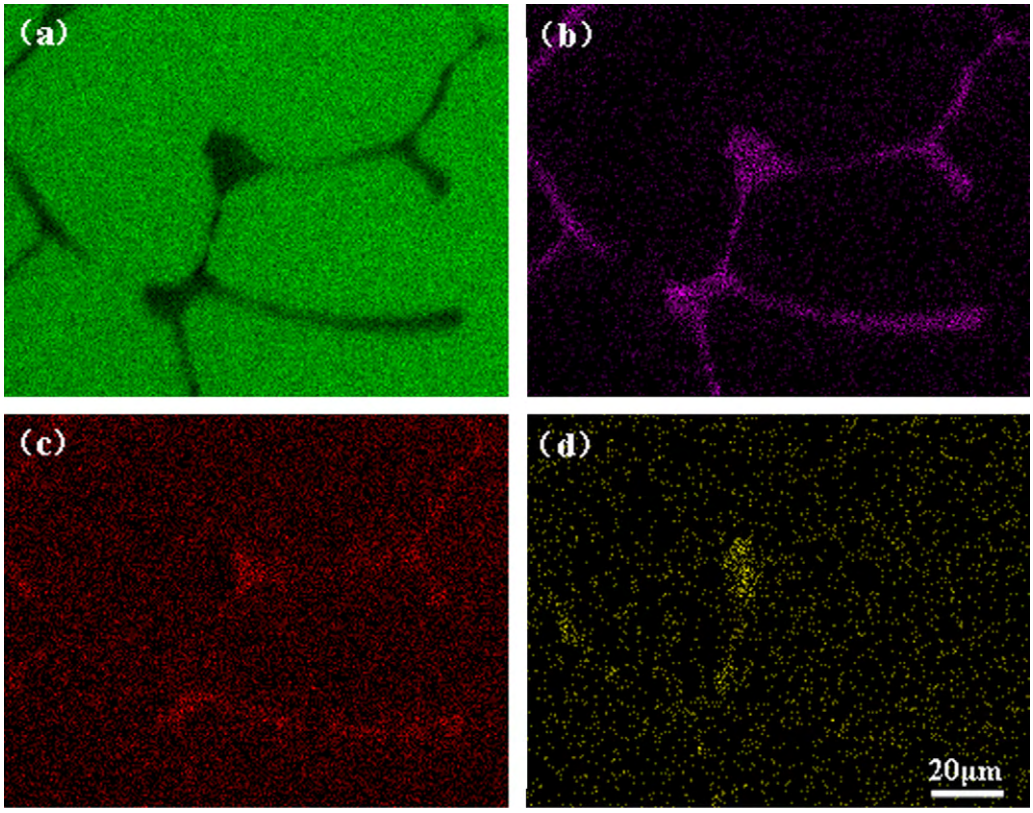

Fig. 4. The elements mapping of as-cast Al–Cu–Mg–Er alloy. (a)Al; (b)Cu; (c)Mg; and (d)Er.

Vickers hardness measurements were carried out in order to investigate the effect of mechanical property with the small addition of erbium. The Vickers hardness value of hot rolled plate of Al–Cu–Mg–Er alloy is slightly lower than that of Al–Cu–Mg alloy [approximately 91 HV versus 98 HV]. As proposed by Nie et al. [2], the Al_2Cu phase as the major hardening constituent is reduced due to the presence of Al_8Cu_4Er in an Al–Cu–Er alloy. The composition of the base alloy just lies in the $(\alpha + \theta + S)$ phase field and the major strengthening phases are θ phase and S phase in the Al–Cu–Mg alloy. Thus, probably it is the presence of primary precipitate (Al_8Cu_4Er phase) that lowers the volume fraction of these major strengthening phases.

3.3. TEM analysis

The bright field TEM image of the Al–Cu–Mg–Er alloy in T351 condition is shown in Fig. 6(a), indicating a type of precipitate with nanoscale formed in the aluminum matrix. In addition, it clearly demonstrates that the precipitates were visible by Ashby-Brown strain field contrast in bright field with the line of no contrast. However, there are also visibile what appear to be dislocations surrounding several of the precipitates, indicating that they are not completely coherent (perhaps only partially coherent). The crystal lattice type and the crystal lattice parameter of Al_3Er precipitates (crystal parameter $a = 0.4215$ nm) are very close to those of aluminum matrix (crystal parameter $a = 0.4049$ nm) and the mismatch is rather small [25], therefore, $A1_3Er$ precipitates are coherent or semi-coherent to the aluminum matrix. In this investigation diffraction patterns revealed the presence of weak reflections of the $L1_2$ structure, as shown in Fig. 6(b). The diffraction spots from the dispersoids can be clearly seen between the relatively large spots from the aluminum matrix. Accordingly, the precipitates with Ashby-Brown type strain contrast could be identified as Al_3Er phases according to the above results and analyses.

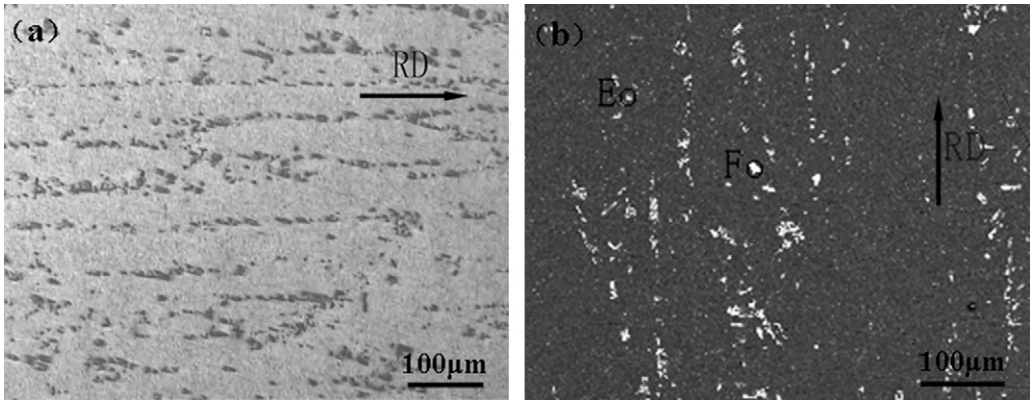

Fig. 5. The optical microstructure (a) [unetched] and BSE image (b) of hot rolling Al–Cu–Mg–Er alloy.

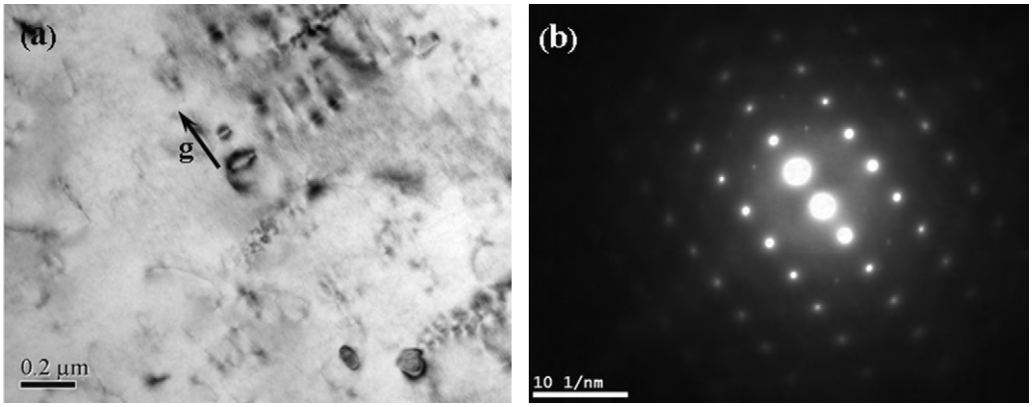

Fig. 6. TEM image of Al–Cu–Mg–Er alloy in T351 condition. (a) Bright field TEM image of the dispersoids; and (b) diffraction image showing an ordered $L1_2$ structure near [1 1 2]-zone.

In an earlier paper, Karnesky et al. [13] revealed that coherent ($L1_2$), near-stoichiometric $Al_3(Sc_{1-x}Er_x)$ precipitates are formed with a core–shell structure in Al–0.06Sc–0.02Er (at.%) alloy, with Sc and Er segregated at the shells and cores, respectively. The formation of $Al_3(Sc_{1-x}Er_x)$ with core–shell structure is attributed to the interfacial free energy between α-Al matrix and Al_3Er phase being larger than that between α-Al and Al_3Sc phases and it is also consistent with the unconstrained lattice parameter misfit between α-Al and Al_3Er being larger than that between α-Al and Al_3Sc [3.0% [26] versus 1.4% [27]]. Considering these observations, it appears that the formation of Al_3Sc phase is much easier than that of Al_3Er phase under the same condition. Similar phenomena has been observed in Ref. [22], where the $Al_3(Sc_{1-x}Zr_x)$ phase was obtained in Al–4.6Cu–0.36Mg–0.11Zr–0.32Sc alloy but there is no Al_3Er phase and $Al_3(Er_{1-x}Zr_x)$ phase was found in Al–4.66Cu–0.39Mg–0.13Zr–0.28Er alloy. However, Karnesky et al. [13] also demonstrated that scandium diffuses faster than erbium in α-Al at 300 °C (the diffusivities are $(6 \pm 3) \times 10^{-20}\ m^2\ s^{-1}$ and $(9 \pm 6) \times 10^{-22}\ m^2\ s^{-1}$, respectively), indicating that erbium may decrease the coarsening kinetics of precipitates in the alloy as compared to scandium. The major existing form of erbium in the as-cast Al–Cu–Mg–Er alloy is Al_8Cu_4Er phase in this study. During solidification, erbium atoms mainly segregate at grain boundary and lead to the formation of ternary Al_8Cu_4Er phase. As can be seen, the grain boundaries were decorated by coarse Al_8Cu_4Er phase in Fig. 4(d) which illustrates the element mapping of erbium in the as-cast Al–Cu–Mg–Er alloy. The equilibrium solid solubility of erbium in aluminum matrix is very low which can be observed from the binary Al–Er alloy phase diagram, but under the experimental condition, the concentration of erbium dissolved in matrix could be improved to a great extent because of a high melting temperature and cooling rate [28]. Those erbium resolved into aluminum matrix can be precipitated in the form of secondary Al_3Er phase during the succedent heating process.

Extensive research has established that nanoscale Al_3Er is a promising precipitate capable of precipitation strengthening and also can inhibit recrystallization [18,20]. The fine secondary Al_3Er particles, precipitated from the supersaturation, anchor the dislocations strongly retarding the motion of the dislocations and improve the shear stress necessary for the dislocations to slide [20].

4. Conclusions

Grain refinement was performed with the small addition of erbium in the as-cast Al–Cu–Mg alloy apparently. Erbium in the Al–Cu–Mg–Er alloy mainly segregated to the grain boundaries during the process of solidification and formed ternary Al_8Cu_4Er phase which was crushed up along with the grain boundaries after hot rolling. Moreover, Al_3Er phase was also observed in the Al–Cu–Mg–Er alloy in T351 condition.

Acknowledgements

Useful discussions with Yanhui Hou (Southwest Jiaotong University) and Chunmei Liu (Xiangtan University) are gratefully acknowledged.

References

[1] W.T. Wang, X.M. Zhang, Z.G. Gao, Y.Z. Jia, L.Y. Ye, D.W. Zheng, L. Liu, J. Alloys Compd. 491 (2010) 366.
[2] Z.R. Nie, J.B. Fu, J.X. Zou, T.N. Jin, J.J. Yang, G.F. Xu, H.Q. Ruan, T.Y. Zuo, Mater. Sci. Forum. 28 (2004) 197.
[3] Y.M. Wu, J. Xiong, R.M. Lai, X.Y. Zhang, Z.X. Guo, J. Alloys Compd. 475 (2009) 332.
[4] S. Bai, Z.Y. Liu, Y.T. Li, Y.H. Hou, X. Chen, Mater. Sci. Eng. A. 527 (2010) 1806.
[5] W.S. Lee, T.H. Chen, C.F. Lin, M.S. Chen, J. Alloys Compd. 493 (2010) 580.
[6] C. Watanabe, R. Monzen, K. Tazaki, Int. J. Fatigue 30 (2008) 635.
[7] M.X. Wang, Z.X. Liu, Z.Y. Liu, S. Yang, Y.G. Weng, T.F. Song, Mater. Sci. Eng. A. 483-484 (2008) 448.
[8] W. Lefebvre, F. Danoix, H. Hallem, B. Forbord, A. Bostel, K. Marthinsen, J. Alloys Compd. 470 (2009) 107.
[9] J. Røyset, N. Ryum, Int. Mater. Rev. 50 (2005) 19.
[10] W.J. Kim, J.K. Kim, H.K. Kim, J.W. Park, Y.H. Jeong, J. Alloys Compd. 450 (2008) 222.
[11] S. Lathabai, P.G. Lloyd, Acta Mater. 50 (2002) 4275.
[12] H. Bo, L.B. Liu, Z.P. Jin, J. Alloys Compd. 490 (2010) 318.
[13] R.A. Karnesky, D.C. Dunand, D.N. Seidman, Acta Mater. 57 (2009) 4022.
[14] A. Ruder, D. Eliezer, J. Mater. Sci. 25 (1990) 3541.
[15] Z.R. Nie, T.N. Jin, J.B. Fu, G.F. Xu, J.J. Yang, J.X. Zhou, T.Y. Zuo, Mater. Sci. Forum. 396-402 (2002) 1731.
[16] M.E. van Dalen, R.A. Karnesky, J.R. Cabotaje, D.C. Dunand, D.N. Seidman, Acta Mater. 57 (2009) 4081.
[17] Z.G. Wu, M. Song, Y.H. He, Mater. Sci. Eng. A. 504 (2009) 183.
[18] S.P. Wen, Z.B. Xing, H. Huang, B.L. Li, W. Wang, Z.R. Nie, Mater. Sci. Eng. A 516 (2009) 42.
[19] S.P. Lin, Z.R. Nie, H. Huang, B.L. Li, Mater. Design. 31 (2010) 1607.
[20] G.F. Xu, S.Z. Mou, J.J. Yang, T.N. Jin, Z.R. Nie, Z.M. Yin, Trans. Nonferrous Met. Soc. China 16 (2006) 598.
[21] J.W. Mao, T.N. Jin, G.F. Xu, Z.R. Nie, Trans. Nonferrous Met. Soc. China 15 (2005) 1341.
[22] Y.T. Li, Z.Y. Liu, Q.K. Xia, Y.B. Liu, Metall. Mater. Trans. A. 38 (2007) 2853.
[23] P. Villars, A. Prince, H Okamoto, Handbook of Ternary Alloy Phase Diagrams [M], ASM International, Materials Park, OH, 1995.
[24] L.G. Zhang, L.B. Liu, G.X. Huang, H.Y. Qi, B.R. Jia, Z.P. Jin, Calphad 32 (2008) 527.
[25] J.J. Yang, Z.R. Nie, T.N. Jin, G.F. Xu, J.B. Fu, H.Q. Ruan, T.Y. Zuo, Trans. Nonferrous Met. Soc. China 13 (2003) 1035.
[26] O.I. Zalutskaya, V.R. Ryabov, I.I. Zalutsky, Dopov. Akad. Nauk. A (1969) 255.
[27] Y. Harada, D.C. Dunand, Mater. Sci. Eng. A. 329-331 (2002) 686.
[28] Z.K. Zhao, T.T. Zhou, P.Y. Liu, C.Q. Chen, Rare Metal Mat. Eng. 33 (2004) 1108.